Wavelet-Based Multiscale Texture Segmentation: Application to Stromal Compartment Characterization on Virtual Slides.

Nicolas Signolle, Marinette Revenu, Benoît Plancoulaine, Paulette Herlin

Wavelet-Based Multiscale Texture Segmentation: Application to Stromal Compartment Characterization on Virtual Slides.

Nicolas Signolle [a,b,*], Marinette Revenu [a], Benoît Plancoulaine [b], Paulette Herlin [b]

[a] *GREYC UMR CNRS 6072 14050 Caen France*

[b] *GRECAN EA 1772, IFR 146 ICORE, Université de Caen, CLCC François Baclesse 3, Avenue du Général Harris 14076 Caen cedex 5 France*

Abstract

We aim at segmenting very large images of histopathology virtual slides with an heterogeneous and complex content. To this end, we propose a multiscale framework for texture-based color image segmentation. The core of the method is based on a wavelet-domain hidden Markov tree model and a pairwise classifiers design and selection. The classifier selection is based on a study of the influence of the hyper-parameters of the method used. Over the testing set, majority vote was found to be the best way of combining outputs of the selected classifiers. The method is applied to the segmentation of various types of ovarian carcinoma stroma, on very large virtual slides. This is the first time such a segmentation is tested. The segmentation results are presented and discussed.

Key words: Segmentation, Texture, Hidden Markov Model, Wavelets, Pairwise classifier combination, Virtual slides

Introduction

To estimate the potential of evolution of cancer lesions, it is often necessary to identify and quantify cell and tissue compartments on histological sections. To perform automatically this measurement in an objective way, an image of the whole tissue preparation must be recorded and fully analyzed, as structures of interest are often heterogeneously spread all over the slide. "Virtual microscopy" devices allow the acquisition and storage of digital images of microscopic structures. When the whole tissue slice is acquired, the recorded image is named "Virtual Slide" (*VS*). Once they have been acquired, virtual slides can then be viewed through the screen of a monitor without using a microscope (Rojo et al., 2006) or automatically analyzed.

It is also mandatory to adapt the working resolution to the size of the structures to be measured. The high resolution *VS* which are recorded for the identification of tiny microscopical structures occupy a considerable volume in memory (several GigaBytes) and cannot be processed at once. Special techniques have to be used to overcome this problem. Recent works suggest to use multi-resolution approaches. The method our team chose is a multiscale analysis of high resolution *VS*, allowing to adapt the working resolution to the various structures to be segmented (i.e. cancer lesion, intra-tumoral tissue compartments, cells and intra-cellular structures).

The present study addresses the segmentation of the various types of stromal compartments on ovarian carcinoma virtual slides. It aims first at partitioning cancer cells and intra-tumoral connective tissue, and then at differentiating the various stromal compartments (fibrous tissue, loose mesenchymatous connective tissue, inflammatory cell accumulation). This work is pioneering in this field.
Each stromal compartment can be identified mainly by its cell shape and organization. This individual pattern can be exploited by a texture-based analysis. It is the way our work focuses on. Furthermore, in order to be easily applied in the anatomopathology laboratories, the method should have a rather low calculation time.

Many studies have already been conducted on the segmentation of textured images. Several categories of methods may be distinguished : the statistical methods which exploit the spatial distribution of the gray levels, the methods based on the construction of a texture model, and the methods which mimic the mechanism of the human vision, integrating several levels of resolution (Xie, 2008, e.g.).

* Nicolas Signolle GREYC - ENSICAEN 6 Boulevard Maréchal Juin 14050 CAEN cedex FRANCE tel : +33 (0)2 31 45 29 20, Fax : +33 (0)2 31 45 26 98

Email address: nicolas.signolle@greyc.ensicaen.fr (Nicolas Signolle).

We chose to use the *Hidden Markov Tree* (HMT) proposed by Crouse (Crouse et al., 1998) as a descriptor because it combines these different approaches. It enables us to make a statistical modeling of intra-scale and inter-scale properties of the coefficients of the wavelet transform (WT) (Mallat, 1999), and it exploits the decorrelation power of this transform. The goal is to capture the inter-scale dependency factor and the non-gaussian distribution of the coefficients computed at each scale. We also use the segmentation proposed by Choi (Choi and Baraniuk, 2001) as a classifier because it allows us to perform texture classification at a range of different scales. Thereby, information collected at coarser-scales guide the segmentation at finer-scale quite in the way the pathologists do.
These tools are used in a framework for the segmention of the various compartments of stroma identified inside VS of ovarian carcinomas, recorded at a high resolution ($0.5\ \mu m$).

The paper is organized as follows : in section 1, we first discuss previous works in the field of large VS segmentation and classification, then, in section 2, due to the complexity and variability of the structures to be segmented, we precisely described the "domain objects" of our images. In section 3, the mathematical background of the used tools is detailed and the results are presented and discussed in section 4 before concluding on the offered prospects.

1. Related work

The analysis of restricted fields of histological slides has long been practiced, but it has been applied only within the past ten years to virtual slides. We will review some solutions proposed in the literature for the segmentation of virtual slides.

One of the first teams that investigated to segment images larger than just a microscopic field is Hamilton's one (Hamilton et al., 1997). They wanted to automatically distinguish the dysplastic tissue from the normal mucosal in colorectal cancer by analyzing texture (using a vector of features, consisting of co-occurrence matrix, run-length matrix, gray level histograms, and then applying a classification rule). The processed images (which size was 3040x2048 pixels) did not yet covered the whole histological slide.

Other teams managed to process an image of the entire slice. The strategies may be grouped into 4 classes: low resolution processing, block processing, multiscale analysis and use of dedicated architectures. These strategies have been used separately or jointly.

1.1. *Processing of the whole image recorded at low resolution*

An image of the whole slice can be obtained at low resolution (from 4000 to 5000 dots per inch). The size of the resulting image (40MB to 100MB) is small enough to allow loading and processing of the whole VS in memory. This strategy was applied to images of the whole histological slide to detect and quantify : blood vessels (Tran et al., 2003; Chantrain et al., 2003), immunolabeled cells (Elie et al., 2003; Mesker et al., 2003) and stromal compartment (Elie et al., 2005). However, low resolution acquisition may be not sufficient to detect tiny structures. This is the reason why high resolution image processing has to be performed.

1.2. *Image processing by blocks*

To avoid to overload the memory, it is possible to cut the image into smaller images and to process them independently. This approach, however, must take into account the associated edge effects. Indeed, structures, cut by the edges of one image, can be detected and counted on several images. An overlapping adapted to the size of the objects to be detected and/or dedicated counting strategies, such as the forbidden line of Gundersen (Gundersen et al., 1988), must be implemented.
The Aperio company, for example, has developed algorithms to quantify nuclear and membrane immunolabeling on 20x recorded images. The image is divided in smaller images of size 1000x1000 with an overlapping of 100 pixels in every direction and forbidden line correction. Although the processing is theoretically possible on the whole image, it is generally applied to areas of interest (Olson, 2006). This approach, however, does not reflect the distribution heterogeneity of structures of interest that is very frequent on tumor sections.
Mete *et al.* used images of 128x128 with an overlapping of 64 pixels to automatically detect tumor foci on 40x virtual slides of malignant cancers of the head and neck (Mete et al., 2007). Mosaliganti *et al.* chose to make a classification of different structures on a slice of mouse embryo from 20x20 pixel patches of a 20X image (Mosaliganti et al., 2008).
Image processing by blocks solves the problem of image size but it doesn't solve the problem of the computing time required when the algorithms get more complex. This is why processing by blocks is often coupled with a multi-resolution analysis.

1.3. *Multi-resolution analysis*

The multi-resolution analysis is based upon the statement that all the details are not essential for the identification of a structure. It is sometimes necessary to reach a certain level of abstraction to process a good segmentation (Signolle et al., 2008). Thus, Ficsor *et al.* proposed to seg-

ment at full resolution the epithelial nuclei of colon cancer, while the glands are detected on an eight time subsampled virtual slide (Ficsor et al., 2008).
He and his team have proposed a multi-resolution strategy in which data are classified at low resolution. The region borders are then refined at a higher resolution (He et al., 2005). Wang and his team have applied a similar method to the segmentation of the squamous epithelium in cancer of the cervix (Wang et al., 2007). The processing time is about 3 hours for a slice of 152,000x42,000 pixels (recorded at 40x) processed by a PC with a 3.4 GHz Pentium IV and 2 GB of RAM. Within the epithelium, areas of intra-epithelial neoplasia are then analyzed (area, density and distribution of the nuclei) at full resolution to classify images of size 250x250 (Wang, 2008).
To separate stroma rich and stroma poor areas in neuroblastoma, Sertel and his team used a weighted k-nearest neighbor classifier at each level of subsampling (Sertel et al., 2009). If an area is classified at any resolution with a confidence index below a chosen threshold, the classification is revised at a higher scale. The more the resolution increases, the more the required level of threshold of the confidence index decreases. This makes the classification fitted to the content of the image and saves about 85 % of computing time.
Kong *et al.* also proposed to use the optimum resolution for classification according to the degree of differentiation of neuroblastoma images (Kong et al., 2007b). If the characteristics calculated for the classification at a given resolution are outside a confidence level predetermined by learning, the analysis is carried on at a higher resolution. The authors noticed that this approach had enabled them to halve the computing time. Kong *et al.*, concerning the same problem, adopted another rule to control the transition between resolutions (Kong et al., 2007a). They determine the class of an area by combining seven different classifiers. Each classifier has a previously learnt confidence index. If the sum of the confidence index of classifiers who voted for the majority class is below a threshold, the analysis is conducted at a higher resolution.

1.4. *Using dedicated architectures*

To reduce the computing time, some authors use a dedicated hardware. A grid of computers (Hastings et al., 2005; Görtler et al., 2006) can be used. Those who cannot afford these devices can use Graphic Processing Units (Hong and Wang, 2004; Ujaldon and Saltz, 2005), of the joint use of processor and GPU (Sertel et al., 2008) or even of a PlayStation 3 (Hartley et al., 2007). Other authors have proposed to employ the specific processor instructions or to create cards dedicated to time consuming operations (Diou et al., 2002).
Among the studies presented above, Kong *et al.* use a grid consisting of 64 nodes for parallel calculations (Kong et al., 2007b; Sertel et al., 2008; Kong et al., 2009). A 75,000x68,000 pixel image is segmented in half an hour, using only 32 of the 64 nodes (Kong et al., 2007a).
By using a grid of 16 multi-processor nodes (Opteron X2 2218) with multi GPU (Quadro FX 5600), Hartley *et al.* obtained the record processing time of 4 seconds for an image of size 33,000x66,000 and 11 seconds for an image of size 110,000x80,000 (both 40x recorded) (Hartley et al., 2007).
Despite these record processing time, beyond the price of the equipment required for a routine pathology department, the major problem of the use of GPU is their low "programmability" (there are few development tools, and they require a good knowledge of the architecture of the card) and the low portability of the written code because of frequent changes in the architecture of the cards.

To summarize, the main approach to tackle large virtual slide segmentation and classification is to process multiscale analysis. This multiscale analysis should be applied to splitted images (tiles) when necessary, but attention has to be paid to the management of tile overlapping. The strategy we adopted takes into account these two points. We process 2048x2048 pixel tiles of the original image with an overlapping of 24 pixels in every direction (these sizes are suited to the resolution and to the size of structures). We chose to use the framework of wavelets to perform a multiscale texture analysis on these tiles.

2. Material

An image can be described considering three levels of description (Renouf et al., 2007):

(i) the physical level that focuses on the characterization of the acquisition system effects on the images.
(ii) the perceptive level that focuses on the description of the visual primitives (regions, lines, ...) without any reference to business objects.
(iii) the semantic level that focuses on the identification of the business objects visualized in the images.

To lay clearly the problem, and to guide the choice of image representation and of segmentation parameters, we will describe the images according to these three levels.

When a patient undergoes surgery for tumour resection, the excised biopsy is fixed in formalin, paraffin embedded and splitted off in 5 μm thick slices. Slices are then affixed on a glass slide prior to be stained. The special staining using immunohistochemistry or histochemistry aims at revealing particular cell types or proteins which amount can then be estimated in order to assess the potential evolution of the tumour and to help choosing the best therapy protocol. In the case of ovarian carcinoma [Fig.1] the prognostic impact of the proportion of stroma is demonstrated (Elie et al., 2005). The researchers need to further clarify the participation of the various stromal compartments in the evolution of tumours and their response to therapy.

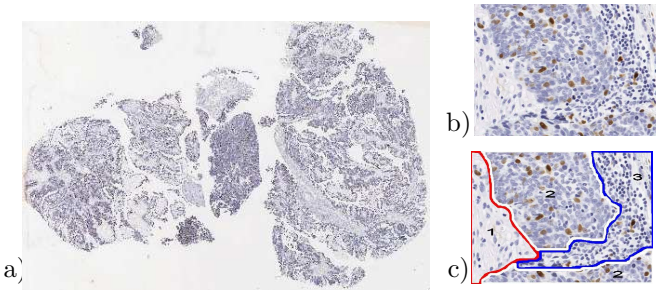

Figure 1. a) Image of an histological section of ovarian carcinoma after DAB immunostaining of proliferation cells (brown) and hematoxylin counterstaining of non proliferating nuclei (blue). The original size of the recorded image is 62000x41404 pixels (acquisition resolution 0.5 μm). b) Detail image. c) Manual drawing of the ideal segmentation of three compartments which can be identified on this detail (1 is loose connective tissue, 2 is cancer cell foci and 3 is inflammatory stromal compartment).

The ovarian carcinoma is made of two types of tissue: cancer epithelial cells and stroma. Stroma refers to the connective tissue which provides supportive framework and nutriments to epithelial cancer cells.
After hematoxylin staining, several types of stromal tissue can be identified inside tumours, some of which corresponding to various maturation degrees: loose connective tissue, cellular stroma and fibrous connective tissue. Inflammatory cell riched foci can also be found [Fig.2].

- The loose connective tissue is an immature stroma. It is made of an abundant extracellular matrix and star shaped mesenchymatous cells. The density of these cells is low. Cell nuclei are small and round.
- The cellular stroma is a young connective tissue. It consists mainly of myofibroblasts organized in sheets and bundles with a high density of cells. The cell nuclei are elongated and plump.
- The fibrous connective tissue is a mature stroma with a density of cells which is somewhat lower than the cellular stroma and a large number of extra-cellular collagen fibers. The nuclei are very thin and elongated. Their optical density is high, due to chromatin condensation.
- The inflammatory stromal compartment is characterized by small round nuclei with a high optical density (lymphocytes and plasma cells) and clover shaped dense nuclei (polymorphonuclear cells).

Extravased red blood cells, necrosis foci and mucus sheets can also be found inside the tumor [Fig.2].
After immunohistochemical staining of proteins associated to cell proliferation (Cyclin A for example), Diaminobenzidin (DAB) labelling of the antibody-antigen reaction and Mayer hematoxylin counterstaining, epithelium appears as blue (non proliferating) and brown (proliferating) cells with large size nucleus [Fig.2]. Nevertheless, with such a staining protocol, the various types of stroma can only be identified thanks to the morphology of their nuclei. Extracellular fibers and matrix are not stained as well.
Finally, we decided to take into account 5 classes : background, epithelial cancer cells, loose connective tissue, cellular stroma and inflammatory stroma.

These descriptions give us valuable information. We can, to some extent, help us with color of the nuclei. Several color components have to be tested to select the best segmentation space(s).
We said that we wanted to use the wavelet framework. The fact that stromal compartments have various density indicates that we should use wavelet filters with various support to characterize them. The various morphology of nucleus will lead us to try wavelets specialists in the detection of details.

Tiled tiff *VS* were recorded at a resolution of $0,5$ μm thanks to a microscopic slide scanner (ScanScope CS from Aperio Technologies) provided with a *20x* objective. A *30%* loss Jpeg compression was applied to each tile when recording images. Uncompressed Images are 3 to 10 GigaBytes files, depending on the scanned tissue area. Images are 60000x40000 pixels large on average.

3. Method description

Our contribution is the design of an operational processing chain based on:

- A multiscale approach,
- The design of specialist classifiers,
- The merging of classification results.

3.1. *Multiscale strategy*

Previous works of our team, based on low resolution analysis strategy (6.3 μm), already allowed to segment and quantify tissue components (quantification of stained nucleus, of epithelium, of blood vessels, of stroma (Tran et al., 2003; Elie et al., 2003)). However, the fine analysis of stroma compartments, which needs a cell to cell discrimination, is impossible at this scale as a cell nucleus is represented by only two or four pixels.

For this purpose, we propose a high resolution analysis strategy. As we have seen previously, the image volume (3 to 10 GB) prevents to process *VS* at once. The tempting solution is to process tiles of a splitted image. But this implies hard constraints on elementary image edges, especially when managing large structures that can be spread over several tiles. Furthermore, large scale structure segmentation can imply local as well as global characteristics which are difficult to take into account. The proposed multiscale approach consists in selecting, at various scales, regions of interest containing objects to be further segmented. This allows the user to adjust the decomposition of the image to its contents. A large structure will be segmented at a low resolution (subsampled image size is then small enough to be held in memory, so that there will be no edge effect to manage). The result of this segmentation will serve as a mask to segment a smaller structure at a higher resolution.

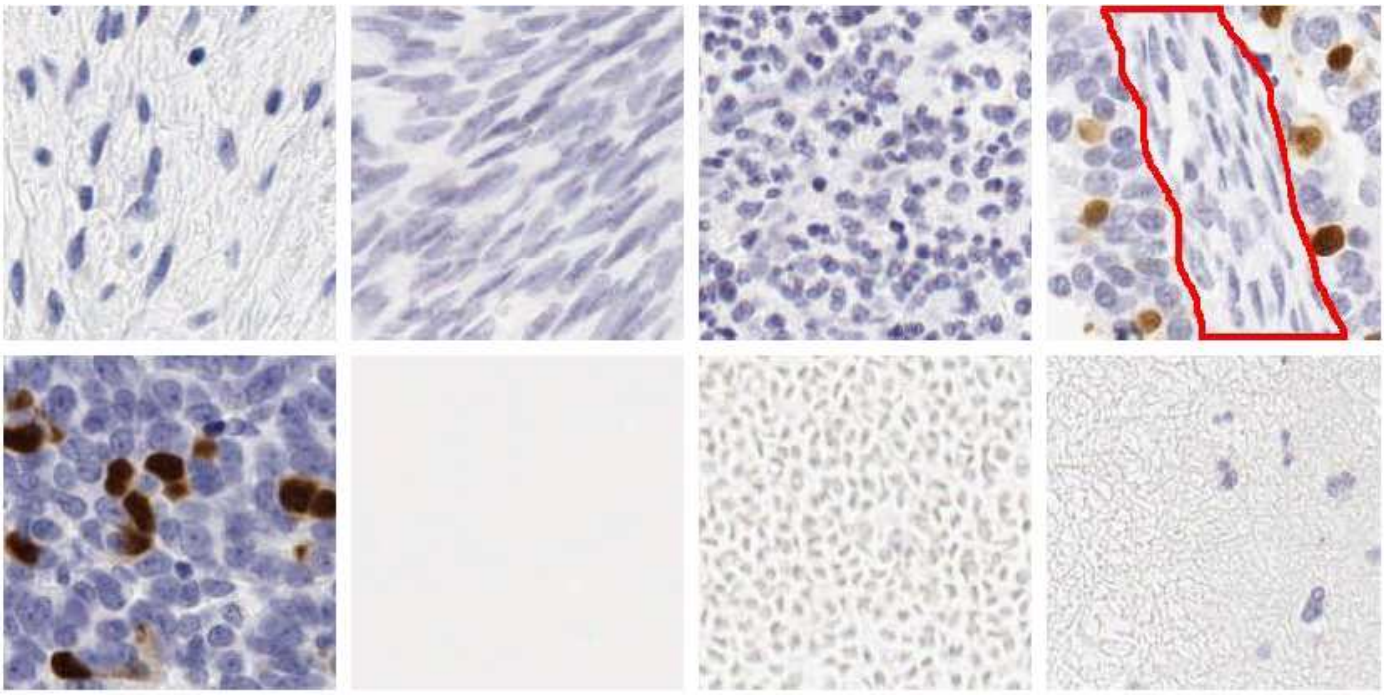

Figure 2. First row (from the left to the right), various types of stroma: loose connective tissue, cellular stroma, inflammatory stroma, and fibrous connective tissue (surrounded area). Second row: other types of tissue compartments encountered in an image of ovarian carcinoma: Epithelial cancer cells, Background, Red Blood Cells, Mucus.

The procedure can be reiterated until the localization of tiny structures inside the full resolution virtual slide.

We use wavelet transform (WT) to subsample the images because we observed that it better preserves the structures and colors than bilinear or bicubic subsampling. A first partitioning between background and tissue can be done at a very low resolution (32 μm) [Fig.3]. For this purpose, the image histogram was regarded as a mixture of three gaussian curves (one mode for background, and two closer modes for stroma and epithelium). The parameters of these three gaussian curves are estimated by an histogram analysis. The likelihood of a pixel to belong to a class (background or tissue) is computed and the image is then segmented by maximum of likelihood. The resulting binary mask of tissue compartment is improved thanks to mathematical morphology operations (hole fill and geodesic opening).

Preliminary tests have been conducted to find the best method to segment the various stromal compartments. The first try aimed at detecting each cell and to analyze the morphology of its nucleus. The difficulty lies in the following fact: at this acquisition resolution, the cells can't be individualized. Therefore, nuclei can't be analyzed. That's why we opted for a more global, texture-based, method. Based texture segmentation methods (such as JSEG criterion (Deng and Manjunath, 2001) or active region based segmentation (Lecellier et al., 2006)) were not able to provide good results of segmentation. Then we choose a method that could combine texture and multiscale analysis : the HMT method.

3.2. *Hidden Markov Tree (HMT) model*

At each scale, the value of coefficients of a wavelet transform depends on the regularity of the signal. A singularity would yield a large coefficient of wavelets that could cascade through scales, while an area with small variation values would produce a series of small coefficients. These properties of the wavelet transform mean that there is a small number of large coefficients bringing most of the energy of the signal, and many small coefficients. To approximate both the marginal and joint wavelet coefficients statistics, Crouse (Crouse et al., 1998) proposed to use a model of Gaussian mixture applied to wavelet coefficients in each sub-band, and a hidden Markov tree (HMT). To each wavelet coefficient, the HMT model associates a (hidden) state variable that controls whether it is Large (L) or Small (S). The joint density of each coefficient is then modeled as a gaussian mixture with a high variance and null average gaussian for the L state and with a low variance one for the S state. The model captures inter-scale dependencies between the wavelet coefficients using a Markov chain, with one dependency between the resolution levels [Fig.4]. This model has been used by Choi (Choi and Baraniuk, 2001) to achieve the segmentation of textured images. The method consists in three phases: a learning phase, a phase of segmentation at each level and a phase of inter-scales merging. During the learning phase, the model parameters $\mathcal{M}$ are learnt for each texture, through an EM (*Expectation Maximization*) algorithm suited to HMT (Crouse et al., 1998): for each state (L or S), each level

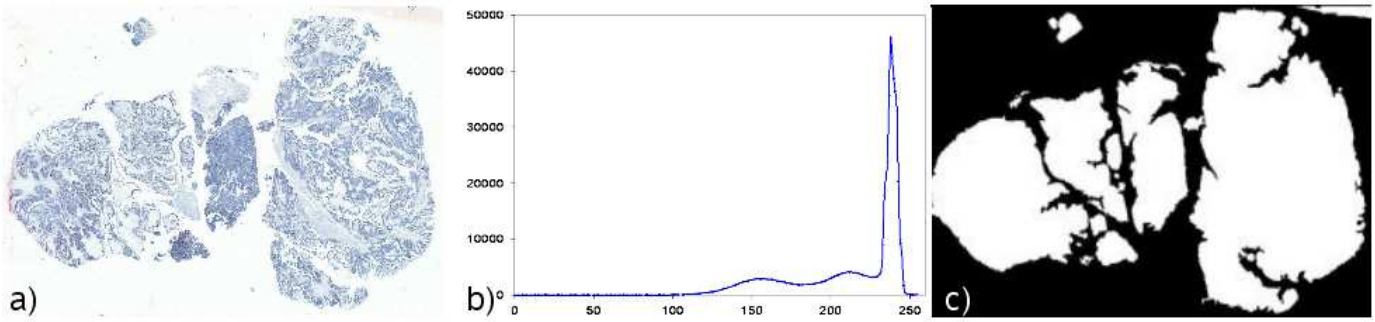

Figure 3. Segmentation of background: a) Original image subsampled 6 times (up to a resolution of 32 μm), b) histogram of the red component of the original coloured image c) segmented background

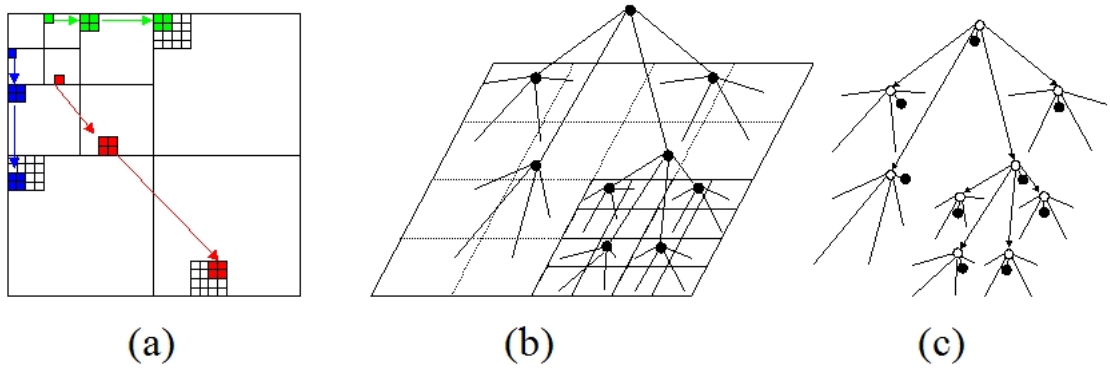

Figure 4. Drawing from (Choi and Baraniuk, 2001) a) The father-son dependencies of WT sub-bands. (b) The quad-tree structure of the model, detailed for a sub-band. (c) The HMT model, detailed for a sub-band. Each wavelet coefficient (black node) is modeled by a gaussian mixture controlled by a hidden state (white node).

and each sub-band, the parameters of the representative Gaussian curves (mean, variance and probability of occurrence) are learnt, as well as the parameters of transition from one state to another, between two resolutions levels: $\begin{bmatrix} \varepsilon_{s=S}^{f=S} & \varepsilon_{s=L}^{f=S} \\ \varepsilon_{s=S}^{f=L} & \varepsilon_{s=L}^{f=L} \end{bmatrix} = \begin{bmatrix} \varepsilon_{s=S}^{f=S} & 1-\varepsilon_{s=S}^{f=S} \\ 1-\varepsilon_{s=L}^{f=L} & \varepsilon_{s=L}^{f=L} \end{bmatrix}$ where $\varepsilon_{s=b}^{f=a}$ represents the probability that the father is in state a while the son is in state b. Details on the implementation of EM algorithm and a proof of convergence are mentioned in (Crouse et al., 1998).
During the phase of segmentation, the likeness between the data of the wavelet transform of the observed image and the HMT model of learnt images is assessed by calculating a likelihood function :

$$f(\mathcal{T}_i|\mathcal{M}) = \prod_{orientations} \sum_{m=S,L} f(\mathcal{T}_i|S_i = m, \mathcal{M}_o) \times p(S_i = m\ |\mathcal{M}_o)$$

where $\mathcal{T}_i$ is a sub-tree of root w_i in one of the sub-bands, $\mathcal{M}_o$ represents the model parameters for a particular orientation and S_i is the hidden state of w_i.
Each pixel is then affected, with the *Maximum of Likelihood* method, to the more similar texture. This yields to a "raw" segmentation at each level.

To improve this first segmentation, the segmentations at different resolutions are subsequently merged. This merging is achieved by maximizing the likelihood of a pixel to belong to a class, taking into account both its value in the raw segmentation and a context vector. This context vector can correspond to the value of the father and of the neighbors of the father (Choi and Baraniuk, 2001), of the neighbors of the son, or a combination of several context vectors (Fan and Xia, 2001) [Fig.5].

3.3. *Design of classifiers*

The HMT parameters are calculated through a learning set of pure class images, for each combination of the method hyper-parameters. Indeed, the HMT model itself can be parameterized : one has to choose the wavelet base (and possibly its order), the color image component on which the WT is applied and the number of resolution levels on which the analysis is focused. These four hyper-parameters can greatly affect the HMT model results.
Each set of hyper-parameters allows us to generate a different segmentation.

Each set of hyper-parameters corresponds to a classifier, and the best of them have to be selected thanks to an evaluation of their performances.
Rather than comparing them for all classes together, we transformed the multiclass problem into a set of bi-

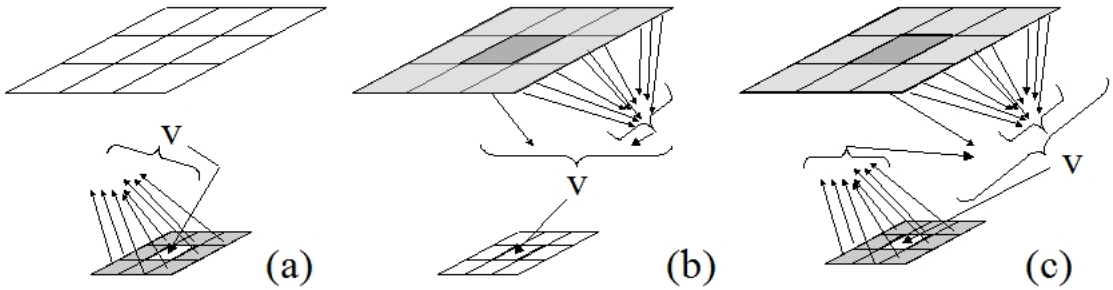

Figure 5. Drawing from (Fan and Xia, 2001). The context vectors V used: a) neighbors of the son (b) neighbors of the father and the fathers value (c) neighbors of the father, sons and fathers value.

nary ones by decomposing it in *one-against-one* problems (Hastie and Tibshirani, 1998).

To evaluate the classifiers, each one is trained to become a discriminative specialist (a dichotomizer) in two classes. For this purpose, we employed a learning base containing images with two classes solely on each image.
HMT segmentation is then performed by suggesting exclusively these two classes as a possible result of segmentation. The classifier which has been kept to distinguish the two classes is the one that maximizes the proportion of well segmented pixels on the two classes compared to the manual drawn "ground truth". This procedure is performed for each pair of classes.
The proportion of well segmented pixels, for each class, represents the confidence attached to the classifier thereafter.

There is so $N = n * (n-1)/2$ binary classifiers (where n is the number of classes). Each classifier uses parameters learnt by the HMT model for one set of hyper-parameters.

3.4. *Merging of each classifier segmentation*

To merge the outputs of the N classifiers, many combination rules can be applied to couple the estimates of each binary classifier in order to obtain class membership estimates for the multi-class problem.
The most commonly used combination rule is probably the *Majority Vote* (Friedman, 1996). Class membership estimates are computed according to the formula:

$$p(\omega = \omega_i|x) = \frac{1}{N} \sum_{j=0, j\neq i}^{N} I(\Psi_{\omega_i,\omega_j}|x) \times Cf(\omega_i, \Psi_{\omega_i,\omega_j})$$

where $\Psi_{\omega_i,\omega_j}|x$ is the probability of segmentation result (class ω_i or ω_j) with classifier Ψ_{ω_i,ω_j} at pixel x. $I(\Psi_{\omega_i,\omega_j}|x)$=1 if $\Psi_{\omega_i,\omega_j}|x = \omega_i$ and 0 otherwise. $Cf(\omega_i, \Psi_{\omega_i,\omega_j})$ is the confidence in Ψ_{ω_i,ω_j} for class ω_i. The resulting label is computed as $argmax(p(\omega|x))$.
One can also use combination rule based on *Error Correcting Output Codes* (*ECOC*) (Dietterich and Bakiri, 1995). Each class is represented by its own output code in the output vector space. The chosen class is the one that is the closest to the 0/1 prediction vector obtained from the classifiers.
The *Loss Based Decoding* (*LBD*) (Allwein et al., 2000) is an improvement of *ECOC* because it allows us to use directly the outputs of the binary classifiers instead of their hard 0/1 predictions.
The comparison of segmentation results with these combination rules is presented below.

To summarize, the method involves two phases. First, large areas of background are discarded at low resolution. Then, the remaining parts of the image are processed as follows (cf. figure 6):
- Parameters and hyperparameters of the HMT method have been learnt for each pair of the K classes, forming a classifier for the classes ω_i and ω_j.
- For each pair of the K classes, the image is segmented, with the HMT method.
- The resulting segmentations are then merged, taking into account the neighborhood of each pixel and the confidence in each one of the classifier.

4. Experimentation and Results

The tests have been conducted with several wavelet bases having various regularity, vanishing moments, support, and symmetry (Haar, Battle Lemarie, Daubechies and bi-orthogonal Splines wavelets were used). Two orders of wavelets (a low one and a high one) are used when possible and one to five levels of HMT subsampling are computed (resulting in four levels of segmentation).
WT is computed on the components of several color spaces ([RGB], normalized [RGB], Excess [RGB] – it is twice red minus green and blue for red component and the same applies for green and blue component–, [HSI], [AC_1C_2] –Garbay's space– [$w_b r_g b_y$] –Ballard's space–, [YCh_1Ch_2] –Caron's space– [$I_1I_2I_3$] –Ohta's space– and PCA components computed from original [RGB]). Scheunders representation is also used. Scheunders (Scheunders, 2003) proposed a method to construct a wavelet representation combining the color plans by computing a coefficient, based on the three values, reflecting their relative importance.
These parameters constitute a total of 576 different segmentations.

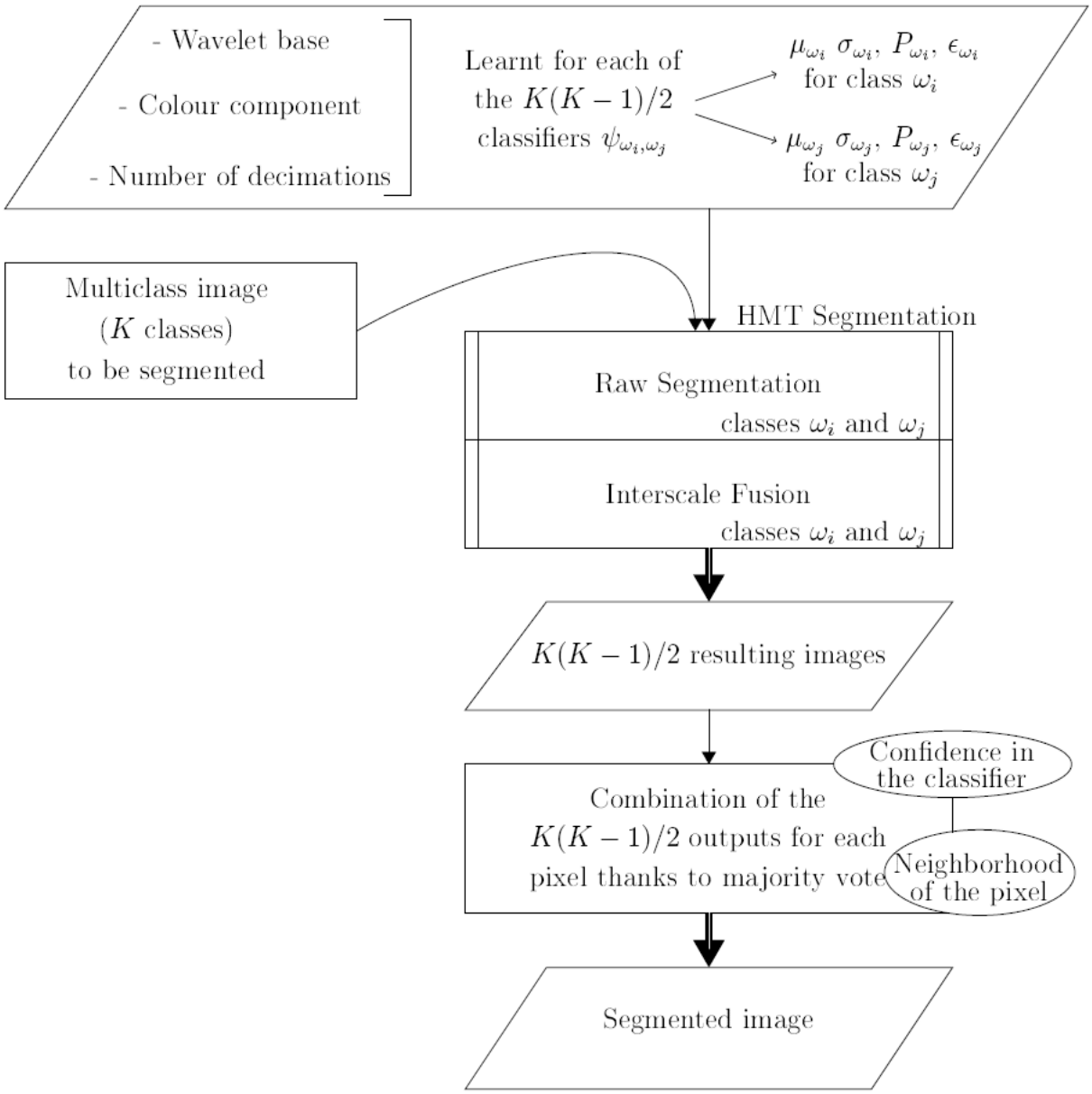

Figure 6. Global schema of the HMT based segmentation method.

HMT training set consists of five 512x512 images of each class. Classifiers are selected on another training set of four 1024x1024 images per pair of classes (*i.e.* 40 images).
The training set has been improved several times, to take into account some variability within the same class, until its images were well segmented by the process.
The resulting hyper-parameters (wavelet base and order, colour component and number of decimation levels taken into account) obtained after selection of the best ones for each pair of classes are summarized in Table 1. Confidence in each classifier for each compartment is indicated too.

To select the best combination rule, a third image set is employed. This testing set is composed of fifteen 2048x2048 images containing all classes in various proportion.

Several combination rules have been tested to merge the binary classifiers : *Error Correcting Output Codes*, *Loss Based Decoding*, but we found that they don't provide any significant improvement over *Majority Vote* (cf. Table 2).

Compared to the reference manual segmentation, 60.05 to 89.67 percent of well labeled pixels are obtained together with correctly localized borders [Fig.7] over the test set using hyper-parameters of table 1 and majority vote. Average is 71.50%. The segmentation result has been improved with further spatial regularization to ban tiny area. The main default is that in some cases, epithelium may be confused with cellular and inflammatory stroma (the closest compartments regarding the texture).

Once the parameters and hyper-parameters of the

Table 1
Parameters allowing good discrimination of compartments. (Epi stands for cancer epithelial cells, CS for cellular stroma, Back for background, LCT for loose connective tissue and IS for inflammatory stroma)

Compartment		Wavelets	Wavelets	color	Level of	Confidence in	
1	2	Base	Order	Component	decimation	compart. 1	compart. 2
LCT	CS	Haar	/	hue	4	96.27	95.30
LCT	Back	Battle	1	i2 (Ohta)	2	99.5	98.97
LCT	IS	Battle	9	normalized green	4	96.29	97.70
LCT	Epi	Splines	5	hue	4	99.35	97.43
CS	Back	Haar	/	Scheunders	1	99.57	99.80
CS	IS	Daubechies	2	excess Green	3	97.62	90.61
CS	Epi	Haar	/	hue	4	97.20	95.97
Back	IS	Daubechies	2	C1 (Garbay)	2	99.38	99.66
Back	Epi	Haar	/	Scheunders	1	99.84	99.81
IS	Epi	Battle	1	hue	4	97.89	98.62

Table 2
Mean and variance percentage of well labeled pixels with various combination rule (ECOC stands for Error Correcting Output Codes, LBD for Loss Based Decoding).

Combination Rule	Majority Vote	ECOC	Weighted ECOC	LBD
Mean % of well labeled pixels (Standard Deviation)	71.50 (12.83)	70.94 (13.33)	71.32 (13.33)	71.22 (13.24)

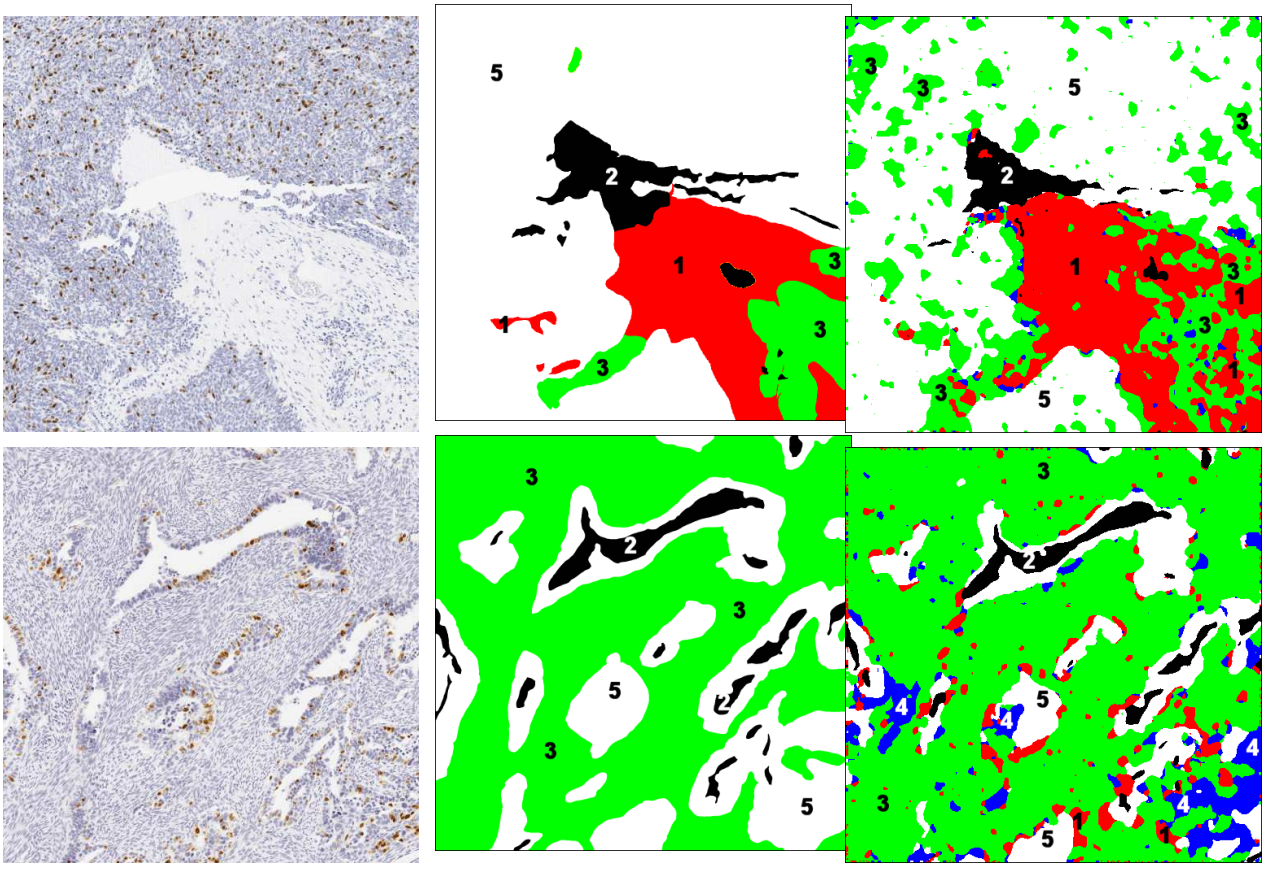

Figure 7. Left : images to be segmented, middle : manual segmentation, right : automated segmentation. 1 is LCT, 2 is Back, 3 is CS, 4 is IS, and 5 is Epi.

method were fixed, tests have then been conducted over 21 images of the whole histological slide [Fig.8]. The size of these images ranges from 38,000x40,000 to 78,000x48,000 pixels. Since drawing manually a ground truth over the whole histological slide is intractable, we chose an other method to validate our results: the stereology (Elias and Hyde, 1983, e.g.). Experts classify the slide exclusively below points regularly spaced. The step between two points is related to the size of structures and is calculated in such a way that the estimated proportions are statistically equivalent to the real proportions. Results of automatic segmentation are compared to this ground truth. First, overall proportions of each compartment of the ground truth and of the calculated image are compared. Then the class of each stereology point of the ground truth is compared to the value of class at the same location on the processed image. The study of results of the automatic segmentation is still going on, but early results seem to be well correlated to the ground truth identified by experts thanks to the stereology test point grid. The results range from 1.14% to 27.72% with an average difference of 8.84% between expert stromal proportion evaluation and the automatic one. These results can currently not be compared to other method results because it is the first time the segmentation of the various types of stromal compartments on ovarian carcinoma virtual slides is tested.

The tests were conducted on a single processor of a 3GHz Xeon quadriprocessor PC. Processing time is from two minutes to one hour per 2048x2048 image, depending on the homogeneity of the image (an image containing only background will be classified quickly while an image with many different regions and singularities will be classified more slowly). Mean time is ten minutes. That is about fifty hours for the processing of a whole 65,000x40,000 Virtual Slide, depending on the amount of background.

Conclusion and Prospects

In the present study, we have investigated a strategy to segment various stromal compartments on ovarian carcinoma virtual slides. No work had ever been published on this topic. The method we proposed is general and could apply to other types of images showing different textures. We suggested to use a wavelet-domain hidden Markov tree model to get classifiers. Selection among these classifiers is done with a *one against one* approach. Classifiers outputs combination is performed thanks to a *Majority Vote* rule. Promising results are obtained on some selected test images and should be confirmed on a larger test set. The ratio of well classified pixels obtained must be appraised taking into account the fact that the transitions between regions of stroma are not clearcut and sometimes difficult to identify even by an expert. Some mislabeling of the epithelium may happen, and the processing time (about fifty hours for a 65,000x40,000 image) due to *Expectation Maximization* algorithm's convergence (from less than 10 to 2000 iterations until convergence, depending on the homogeneity of the processed image) is prohibitive for any clinical use.
To answer the problem of cancer cells foci detection, we plan to use, first, previously described methods (Elie et al., 2003) to locate epithelium at a low resolution and to eliminate it from the higher resolution analysis. We could also employ this low resolution segmentation as an a priori for the higher resolution segmentation.
To cope with the processing time, we have to optimize our code and consider replacing EM part with a faster converging method. We plan also to study other segmentation approaches including image patch exemplar based methods. Finally, our algorithm (or parts of it) could be implemented in specific hardware for parallelisation.

Acknowledgments

This work is funded by a BDI grant cofinanced by the CNRS and the Regional Council of Lower Normandy.

References

Allwein, E. L., Schapire, R. E., Singer, Y., 2000. Reducing multiclass to binary: A unifying approach for margin classifiers. Journal of Machine Learning Research 1, 113–141.

Chantrain, C. F., Declerck, Y. A., Groshen, S., Mcnamara, G., February 2003. Computerized quantification of tissue vascularization using high-resolution slide scanning of whole tumor sections. The Journal of Histochemistry & Cytochemistry 51 (2), 151–158.

Choi, H., Baraniuk, R., 2001. Multiscale image segmentation using wavelet-domain hidden Markov models. IEEE Transactions on Image Processing 10 (9), 1309–1321.

Crouse, M. S., Nowak, R., Baraniuk, R., 1998. Wavelet-based statistical signal processing using hidden Markov models. IEEE Transactions on Signal Processing 46, 886–902.

Deng, Y., Manjunath, b., 2001. Unsupervised segmentation of color-texture regions in images and video. IEEE Transactions on Pattern Analysis and Machine Intelligence 23 (8), 800–810.

Dietterich, T. G., Bakiri, G., 1995. Solving multiclass learning problems via error-correcting output codes. Journal of Artificial Intelligence Research 2, 263–286.

Diou, C., Torres, L., Robert, M., Sassatelli, G., Juillet 2002. Intgration d'une architecture rcursive sur silicium pour la transforme en ondelettes 2D. Traitement du Signal 19 (2), 101–117.

Elias, H., Hyde, D. M., 1983. A guide to practical stereology. Karger Continuing Education Series, 305 pages.

Elie, N., Labiche, A., Michels, J.-J., Herlin, P., June 2005. Control of low-resolution scanning of ovarian tumor stro-

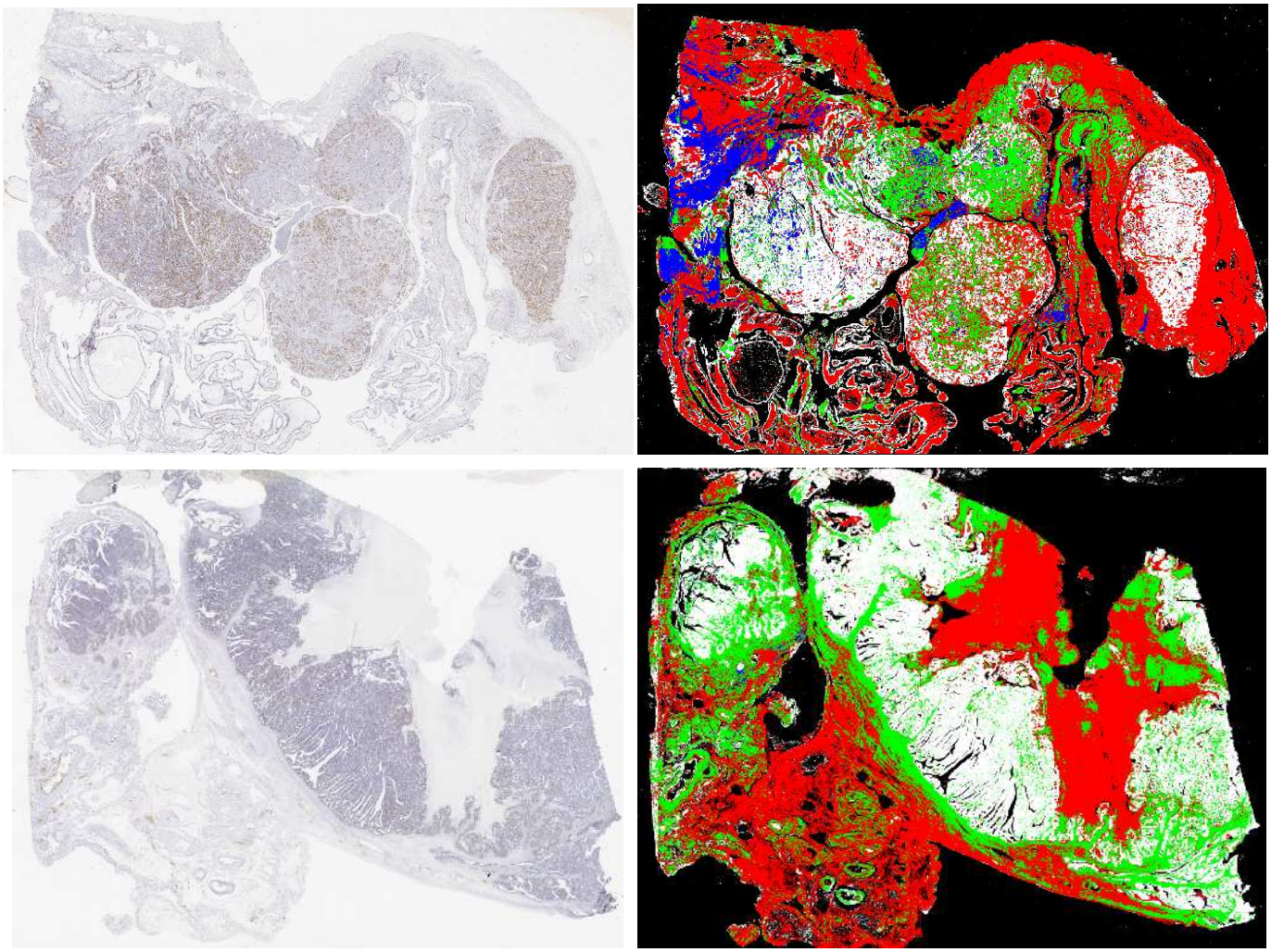

Figure 8. Automated segmentation of two whole slides

mal compartment. Image Analysis and Stereology 24, 85–93.

Elie, N., Plancoulaine, B., Signolle, J.-P., Herlin, P., November 2003. A simple way of quantifying immunostained cell nuclei on the whole histologic section. Cytometry 56A, 37–45.

Fan, G., Xia, X.-G., 2001. A joint multicontext and multiscale approach to bayesian segmentation. IEEE Transactions on Geoscience and Remote Sensing 39 (12), 2680–2688.

Ficsor, L., Varga, V. S., Tagscherer, A., Tulassay, Z., Molnar, B., March 2008. Automated classification of inflammation in colon histological sections based on digital microscopy and advanced image analysis. Cytometry Part A 73A (3), 230–237.

Friedman, J. H., 1996. Another approach to polychotomous classification. Tech. rep., Department of Statistics, Stanford University.

Görtler, J., Berghoff, M., Kayser, G., Kayser, K., August 2006. Grid technology in tissue-based diagnosis: Fundamentals and potential developments. Diagnostic Pathology 1 (1), 23.

Gundersen, H. J., Bendtsen, T. F., Korbo, L., Marcussen, N., Nyengaard, J. R., Pakkenberg, B., Sørensen, F. B., Vesterby, A., 1988. Some new, simple and efficient stereological methods and their use in pathological research and diagnosis. Acta Pathologica, Microbiologica et Immunologica Scandinavica 96 (5), 379–394.

Hamilton, P. W., Bartels, P. H., Thompson, D., Anderson, N. H., Montironi, R., Sloan, J. M., May 1997. Automated location of dysplastic fields in colorectal histology using image texture analysis. The Journal of Pathology 182 (1), 68–75.

Hartley, T. D., Sertel, O., Khan, M., Çatalyürek, Ü. V., Saltz, J. H., Gurcan, M. N., 2007. Neuroblastoma stroma classification on the Sony PlayStation 3. In: APIII07, The Advancing Practice, Instruction, and Innovation through Informatics Conference on Anatomic Pathology Informatics and Imaging Support for Translational Medicine. Pittsburgh, United States.

Hastie, T., Tibshirani, R., 1998. Classification by pairwise coupling. Annals of statistics 26 (2), 451–471.

Hastings, S., Oster, S., Langella, S., Kurc, T. M., Pan, T., Çatalyürek, Ü. V., Saltz, J. H., May 2005. A grid-based

image archival and analysis system. Journal of the American Medical Informatics Association 12 (3), 286–295.

He, Y., Zhang, B., Li, J., 2005. A new multiresolution classification model based on partitioning of feature space. In: IEEE International Conference on Granular Computing. Vol. 3. Beijing, China, pp. 462–467.

Hong, J. Y., Wang, M. D., 2004. High speed processing of biomedical images using programmable GPU. In: ICIP04 : Proceedings of the International Conference on Image Processing. Singapore, pp. 2455–2458.

Kong, J., Sertel, O., Shimada, H., Boyer, K. L., Saltz, J. H., Gurcan, M. N., 2007a. Computer-aided grading of neuroblastic differentiation: Multi-resolution and multi-classifier approach. In: ICIP07, International Conference on Image Processing. Vol. 5. San Antonio, Texas, USA, pp. 525–528.

Kong, J., Sertel, O., Shimada, H., Boyer, K. L., Saltz, J. H., Gurcan, M. N., 2009. Computer-aided evaluation of neuroblastoma on whole-slide histology images: Classifying grade of neuroblastic differentiation. Pattern Recognition 42 (6), 1080–1092, digital Image Processing and Pattern Recognition Techniques for the Detection of Cancer.

Kong, J., Shimada, H., Boyer, K. L., Saltz, J. H., Gurcan, M. N., 2007b. A new multi-resolution analysis framework for classifying grade of neuroblastic differentiation. Tech. rep., Ohio State University.

Lecellier, F., Jehan-Besson, S., Fadili, J., Aubert, G., Revenu, M., Saloux, E., 2006. Region-based active contour with noise and shape priors. In: ICIP06, Proceedings of the International Conference on Image Processing. Atlanta, Georgia, USA, pp. 1649–1652.

Mallat, S., 1999. A wavelet tour of signal processing. Academic Press, 620 pages.

Mesker, W. E., Doekhie, F. S., Vrolijk, H., Keyzer, R., Sloos, W. C. R., Morreau, H., O'Kelly, P. S., de Bock, G. H., Tollenaar, R. A. E. M., Tanke, H. J., 2003. Automated analysis of multiple sections for the detection of occult cells in lymph nodes. Clinical Cancer Research 9 (13), 4826–4834.

Mete, M., Xu, X., Fan, C.-Y., Shafirstein, G., 2007. Automatic delineation of malignancy in histopathological head and neck slides. In: MCBBS07, Proceedings of the Fourth Annual MidSouth Computational Biology and Bioinformatics Society : Conference. Computational Frontiers in Biomedicine. Vol. 8, Supplment 7 of BMC Bioinformatics. New Orleans, United States, abstract S17.

Mosaliganti, K., Pan, T., Ridgway, R., Sharp, R., Cooper, L., Gulacy, A., Sharma, A., Irfanoglu, O., Machiraju, R., Kurc, T., de Bruin, A., Wenzel, P., Leone, G., Saltz, J. H., Huang, K., December 2008. An imaging workflow for characterizing phenotypical change in large histological mouse model datasets. Journal of Biomedical Informatics 41 (6), 863–873.

Olson, A. H., 2006. Image analysis using the Aperio ScanScope. Tech. rep., Aprio Technologies.

Renouf, A., Clouard, R., Revenu, M., 2007. How to formulate image processing applications ? In: ICCVS07, Proceedings of the International Conference on Computer Vision Systems. Bielefeld, Germany, p. 10.

Rojo, M. G., Garca, G. B., Mateos, C. P., Garca, J. G., Vicente, M. C., October 2006. Critical comparison of 31 commercially available digital slide systems in pathology. International Journal of Surgical Pathology 14 (4), 285–205.

Scheunders, P., 2003. An orthogonal wavelet representation of multivalued images. IEEE Transactions on Image Processing 12 (6), 718–725.

Sertel, O., Kong, J., Lozanski, G., Shana'ah, A., Çatalyürek, Ü. V., Saltz, J. H., Gurcan, M. N., 2008. Texture classification using nonlinear color quantization: Application to histopathological image analysis. In: ICASSP08, Procedings of the IEEE International Conference on Acoustics, Speech and Signal Processing. Las Vegas, United States, pp. 597–600.

Sertel, O., Kong, J., Shimada, H., Çatalyürek, Ü. V., Saltz, J. H., Gurcan, M. N., 2009. Computer-aided prognosis of neuroblastoma on whole-slide images: Classification of stromal development. Pattern Recognition 42 (6), 1093–1103, digital Image Processing and Pattern Recognition Techniques for the Detection of Cancer.

Signolle, N., Plancoulaine, B., Herlin, P., Revenu, M., 2008. Texture-based multiscale segmentation: Application to stromal compartment characterization on ovarian carcinoma virtual slides. In: 3rd International Conference on Image and Signal Processing. Vol. 5099 of Lecture Notes in Computer Science. Springer, pp. 173–182.

Tran, K., Elie, N., Plancoulaine, B., Herlin, P., Coster, M., 2003. An original approach for quantification of blood vessels on the whole tumour section. Analytical Cellular Pathology 25 (2), 63–75.

Ujaldon, M., Saltz, J. H., 2005. The GPU on irregular computing: Performance issues and contributions. In: CADCG05, Proceedings of the Ninth International Conference on Computer Aided Design and Computer Graphics. Hong Kong, pp. 442–450.

Wang, Y., April 2008. Computer assisted diagnosis of cervical intraepithelial neoplasia (cin) using histological virtual slides. Ph.D. thesis, School of Electronics, Electrical Engineering and Computer Science, Queen's University, Belfast, United Kingdom.

Wang, Y., Turner, R., Crookes, D., Diamond, J., Hamilton, P., 2007. Investigation of methodologies for the segmentation of squamous epithelium from cervical histological virtual slides. In: IMVIP07, Proceedings of the 7th International Machine Vision and Image Processing Conference. Maynooth, Ireland, pp. 83–90.

Xie, X., 2008. A review of recent advances in surface defect detection using texture analysis techniques. Electronic Letters on Computer Vision and Image Analysis 7 (3), 1–22.